Reachability Conditions of UAVs Net Recovery Based on Pseudo-Spectral Methods

MA Hai-Biao, DU Guang-Xun, ZHANG Hui, QUAN Quan
School of Automation Science and Electrical Engineering
Beihang University
Beijing 100191, P.R.China
Email: mhb_forever@163.com, dgx@buaa.edu.cn, victorzhang@ecpk.buaa.edu.cn, qq_buaa@buaa.edu.cn

***Abstract*—Net recovery is an advanced accurate-point recovery way for small fixed-wing unmanned aerial vehicles (UAVs), especially in limited recovery fields or naval vessels. In order to perform recovery successfully, the aerial vehicle must satisfy certain conditions to shut down the engine so that it can glide into the net without a crash. In this paper, an aircraft longitudinal dynamic model is taken into consideration. Given the initial position, we aim to obtain the feasible initial speed of the aircraft. This problem is formulated as an optimal control problem and then solved by Pseudo-Spectral methods. The simulation results show the initial state in the computational flight envelope can perform successful net recovery task.**

***Keywords*—UAV; Net recovery; Reachability Conditions; Optimal control; Pseudo-Spectral-Methods**

I. Introduction

Unmanned aerial vehicles (UAVs) have been extensively studied in recent years due to their importance on surveillance, product deliveries, aerial photography and agriculture. Fixed-wing UAVs have been considerably researched with its advantages of long endurance and high maneuverability. Most UAVs will be recycled and reused in different ways after executing task. The net recovery technology provides an advanced accurate-point recovery method for small fixed-wing UAVs, especially in limited recovery fields or naval vessels. However, the UAV recovery process is more prone to fail due to various factors and the consequence is serious, which suggests that safety should be considered primarily.

Because of the large advantages of net recovery, there has been extensive research about the net recovery system as well as the control strategy. Kim et al. [1] developed an autonomous vision-based net recovery system for small fixed-wing UAVs where the overall construction processes were all discussed in detail, and the experimental result showed the autonomous capabilities including take-off, waypoint following and vision-based net recovery. Yoon et al. [2] presented a pursuit guidance law and a nonlinear controller for a vision-based net-recovery UAV instead of tracking the pre-designed glide slope, and the constrained adaptive backstepping controller overcame a sudden wind gust in the landing. Robert et al. [3] utilized single-frequency carrier-phase differential GNSS to achieve autonomous net recovery of fixed-wing UAVs. Maya et al. [4] solved maximum gliding range in the event of engine cut-off, which can be used to evaluate a safe landing in a specific landing zone. Although there are many studies on UAVs net recovery, the reachability conditions have received surprisingly little attention. In fact, the aircraft must satisfy certain conditions and then shut down the engine to perform recycling task. Otherwise, it will lead to failure. In these conditions that aircraft need to satisfy, namely reachability conditions, constraints on speed particularly play an important role. Reachability conditions for UAVs net recovery are complex nonlinear optimal control problems, subject to state constraints and control constraints. It has been spent enormous effort on developing computational methods for finding accurate solutions of optimal control problems. Pseudo-Spectral-Method is a kind of direct collocation method which has become popular in nonlinear optimal control problems, e.g. [5]-[7]. In addition, the toolbox GPOPS in software MATLAB® is based on hp-adaptive pseudo-spectral for solving complex optimal control problems [8]-[12]. Therefore, the toolbox provides a convenient way to solve the optimal control problem of using pseudo-spectral methods.

The purpose of current study is to explore the reachability conditions of small fixed-wing UAVs for safe net recovery. This paper is focused on optimizing the appropriate initial speed envelope. By considering an aircraft longitudinal dynamic model, the problem is formulated as an optimal control problem and then successfully solved based on Pseudo-Spectral methods by utilizing GPOPS toolbox.

This paper is organized as follows. In Sec. II, an overview of the net-recovery system architecture is presented. In Sec. III, a longitudinal nonlinear dynamic model of the unmanned aerial vehicle is built based on three assumptions, and the problem is analyzed and formulated. In Sec. IV, the formulated problem is solved based on the pseudo-spectral method by utilizing GPOPS toolbox. Sec. V performs simulated verification, and simulation results demonstrate that the computational reachability conditions are significantly effective. Finally, Sec. VI gives a brief summary and concludes the paper.

II. Brief Description of Net Recovery

A widely used method for UAV net recovery is the vision-based landing system. As shown in Fig. 1, the vision system consists of three parts: Vision Sensors, Image Processing Unit and Estimation Module. The vision system captures the recovery net and delivers the processed information (usually contains altitude and distance relative to the aerial vehicle)

978-1-5386-3524-7/17/$31.00 ©2017 IEEE

to path planner. Also, the aerial vehicle transmits its location information to path planner. The path planner consolidates all information and designs the desired trajectory which can be a guide to the aerial vehicle to reach the recovery net safely.

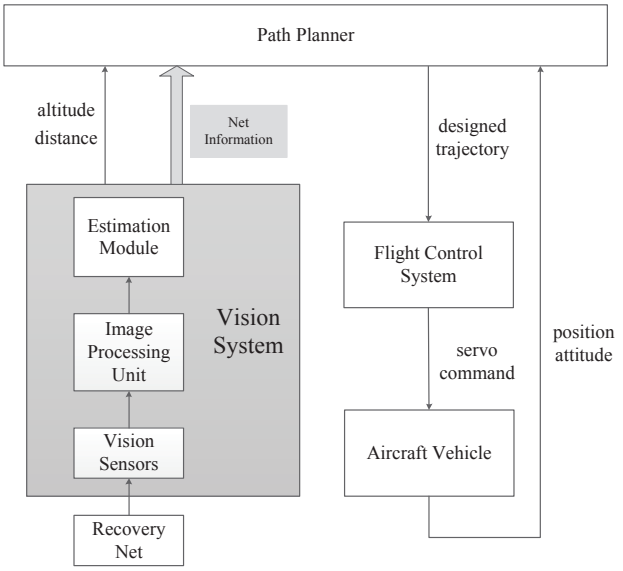

Fig. 1. Vision-Based Net-Recovery system architecture

However, there is no doubt that not all flight conditions can design a desired trajectory successfully due to constraints on aircraft performance. In general, the aircraft will evaluate the error between current state and the reachability conditions and then adjust the flight state accordingly until it is satisfied. After that, the aircraft will shut down the engine and the path planner will design a trajectory in the meanwhile. Finally, the aircraft will track the pre-designed trajectory until landing on the recovery net. However, the aircraft sometimes may trap into the dead zone where the vehicle cannot perform successful net recovery no matter how to adjust flight state, and this situation indicates a failure of the mission (see Fig. 2).

Therefore, the reachability conditions are of great importance during the net recovery process. Solving the reachability conditions can be safer and more reliable to accomplish the recovery task.

III. Problem Formulation

A. Aircraft Model

To analyze the reachability conditions of an unmanned aerial vehicle in the event of engine shut-down, for simplicity, three assumptions are given:

Assumption 1 : The aerial vehicle has the conventional configuration, which means that it is symmetric about the plane spanned by axis x_b and z_b. In this situation, the inertial products of the vehicle J_{xy}=J_{yz}=0.

Assumption 2 : The aerial vehicle is in the state of level and non-sideslipping flight after the engine is shut down, which implies that $\phi = \beta \equiv 0$ and $r = p \equiv 0$.

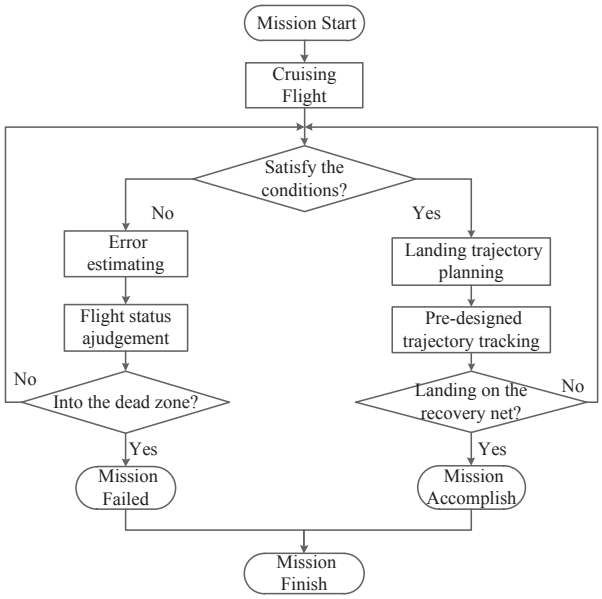

Fig. 2. Flow diagram of net-recovery process

Assumption 3 : The impact of the wind on the aerial vehicle is ignored.

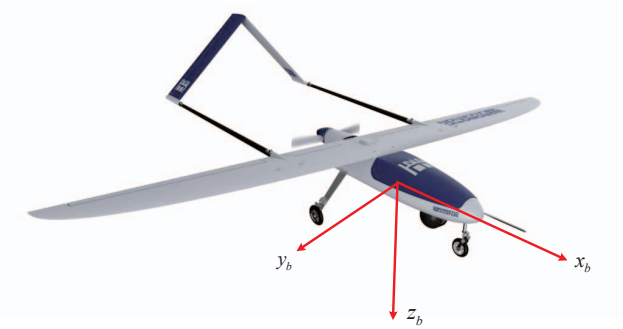

Fig. 3. Aerosonde UAV

Based on the three assumptions, the longitudinal motion of the aerial vehicle after the engine shutting down is only considered. The aircraft model can be represented by the following abstract expression:

$$\dot{\mathbf{x}}(t) = f(\mathbf{x}, \mathbf{u}, t) \tag{1}$$

where $\mathbf{x}(t) \in R^n$ is the system state, $\mathbf{u}(t) \in [a, b]^m \in R^m$ is the control input. In this paper, the dynamic model of the aerial vehicle is described by six equations of motion. The system state is $\mathbf{x} = [x\ h\ u_r\ w_r\ \theta\ q]^T$, where the six state variables represent x-position (m), z-position (m), x-velocity (m/s), z-velocity (m/s), pitch angle (rad) and pitch rate (rad/s) respectively. The control input is elevator deflection δ_e.

The kinematics equations of the aerial vehicle can be represented as

$$\begin{bmatrix} \dot{x} \\ \dot{h} \end{bmatrix} = \begin{bmatrix} \cos\theta & \sin\theta \\ \sin\theta & -\cos\theta \end{bmatrix} \begin{bmatrix} u_r \\ w_r \end{bmatrix} \quad (2)$$

The dynamics equations of the aerial vehicle can be represented as

$$\dot{u}_r = -qw_r - g\sin\theta + \frac{1}{m}\left(-F_{drag}\cos\alpha - F_{lift}\sin\alpha\right) \quad (3)$$

$$\dot{w}_r = qu_r + g\cos\theta + \frac{1}{m}\left(-F_{drag}\sin\alpha + F_{lift}\cos\alpha\right) \quad (4)$$

where α is the angle of attack, m is the mass of the aerial vehicle, F_{drag} and F_{lift} represent the drag and lift forces respectively. The drag and lift forces are heavily influenced by the angle of attack α. The pitch rate q and the elevator deflection δ_e also influence the longitudinal forces and moment. Therefore, the drag and lift forces can be represented by

$$F_{lift} = \frac{1}{2}\rho V_a^2 S\left(C_L(\alpha) + C_{L_q}q + C_{L_{\delta_e}}\delta_e\right) \quad (5)$$

$$F_{drag} = \frac{1}{2}\rho V_a^2 S\left(C_D(\alpha) + C_{D_q}q + C_{D_{\delta_e}}\delta_e\right) \quad (6)$$

where ρ is the air density, S is the planform area of the aerial vehicle wing, V_a is the speed of the aerial vehicle through the surrounding air mass, and the coefficients $C_{L_q} \triangleq \frac{\partial C_L}{\partial q}, C_{L_{\delta_e}} \triangleq \frac{\partial C_L}{\partial \delta_e}, C_{D_q} \triangleq \frac{\partial C_D}{\partial q}, C_{D_{\delta_e}} \triangleq \frac{\partial C_D}{\partial \delta_e}$ are dimensionless quantities. A lift model that incorporates the common linear lift behavior and the effect of stall is given by [13]

$$C_L(\alpha) = (1-\sigma(\alpha))(C_{L_0} + C_{L_\alpha}\alpha) + \sigma(\alpha)\left(2sign(\alpha)\sin^2\alpha\cos\alpha\right) \quad (7)$$

where

$$\sigma(\alpha) = \frac{1 + e^{-M(\alpha-\alpha_0)} + e^{M(\alpha+\alpha_0)}}{\left(1+e^{-M(\alpha-\alpha_0)}\right)\left(1+e^{M(\alpha+\alpha_0)}\right)} \quad (8)$$

and the coefficients M and α_0 are positive constants. A drag model that combines the common parasitic drag and the induced drag is given by [13]

$$C_D(\alpha) = C_{D_p} + \frac{(C_{L_0} + C_{L_\alpha}a)^2}{\pi e AR} \quad (9)$$

where $AR \triangleq b^2/S$ is the wing aspect ratio, b is the wingspan, the parameter e is the Oswald efficiency factor ranging between 0.8 and 1.0, and C_{D_p} is roughly constant denoting parasitic drag.

Due to the fact that the aerial vehicle is in the state of level and non-sideslipping flight, which means $\phi = \beta \equiv 0$ and $r = p \equiv 0$. Therefore we have

$$\dot{\theta} = q \quad (10)$$

and

$$\dot{q} = \frac{1}{J_y}m_p \quad (11)$$

where J_y is the moment of inertia around the y axis and m_p is pitching moment.

Similar to the drag and lift forces, approximation for the pitching moment can be represented as

$$m_p = \frac{1}{2}\rho V_a^2 Sc\left(C_{m_0} + C_{m_\alpha}\alpha + C_{m_q}q + C_{m_{\delta_e}}\delta_e\right) \quad (12)$$

where c is the mean chord of the aircraft wing, and the coefficients $C_{m_\alpha} \triangleq \frac{\partial C_m}{\partial \alpha}, C_{m_{\delta_q}} \triangleq \frac{\partial C_m}{\partial \delta_q}, C_{m_{\delta_e}} \triangleq \frac{\partial C_m}{\partial \delta_e}$ are dimensionless quantities.

The aircraft longitudinal motion equations (2)(3)(4)(10)(11) describe dynamic properties of the defined six states $\mathbf{x} = [x\ h\ u_r\ w_r\ \theta\ q]^T$, and they constitute abstract expression (1) namely the aircraft model. The defined plane-coordinates system is shown as follows: the position of recovery net is set to the coordinate origin o_g, the axis $o_g x_g$ points to flying direction and the axis $o_g z_g$ is perpendicular to axis $o_g x_g$ pointing upside (see Fig. 4).

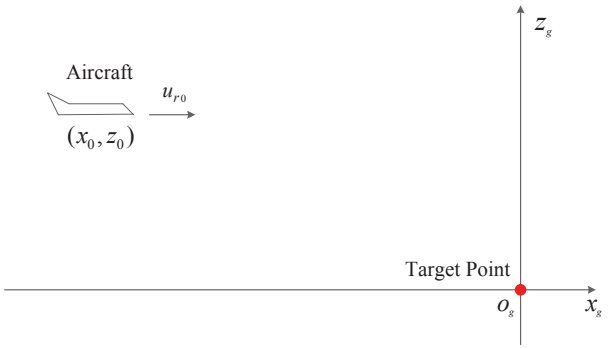

Fig. 4. The coordinates system

The aircraft model established above is a generic model. In order to carry out simulation experiments, this paper utilized the physical parameters of Aerosonde UAV (see Fig. 3), and its primary parameters are described in [13].

B. Problem Formulation

The aerial vehicle cannot reach the target area if the initial speed is too low, while it would suffer destruction with high speed because of impact force. Therefore, in order to ensure the vehicle can reach the target area safely under the condition of no power, the initial speed of the vehicle should be limited to a certain range at the different position.

As mentioned above, the initial speed is the optimal target. Here, we consider the initial speed of $o_g x_g$ direction namely u_{r_0}. To solve the minimum speed, u_{r_0} is minimized. Therefore, minimize the cost functional

$$J_1 = u_{r_0} \quad (13)$$

subject to the dynamic constraint (1) and the control constraint

$$u \in [u_{\min}, u_{\max}] \quad (14)$$

In order to make sure the vehicle land safely, u_r is confined to 1 m/s at the end of the net-recovery phase. Based on the

assumption 2, given the initial position (x_0, h_0) of the aircraft, the cost functional is also subject to the boundary conditions

$$w_r(0) = 0, \quad \theta(0) = 0, \quad q(0) = 0, \quad u_r(t_f) = 1 \tag{15}$$

$$x^2(t_f) + h^2(t_f) \leq \varepsilon \tag{16}$$

where t_f is terminal time of the whole task, subject to time constraint $t_f \in [t_{f\min}, t_{f\max}]$; $x(t_f)$ and $h(t_f)$ represent the position of aircraft at the terminus of the whole task; ε is a constant, which is related to the geometric dimension of the net. In other words, expression (16) implies a successful net recovery behaviour.

On the other hand, u_{r_0} reaches the maximum when $-u_{r_0}$ is minimized. Therefore, minimize the cost functional

$$J_2 = -u_{r_0} \tag{17}$$

subject to dynamic constraint (1), control constraint(14) and boundary conditions (15)(16).

Hereto, the problem about solving the reachability conditions has been formulated as an optimal control problem.

IV. Simulation Results

As described above, the initial speed is an important factor affecting the success of the net recovery. The reachability conditions are the flight envelope established by the maximum speed envelope and the minimum speed envelope. The algorithm of solving the reachability conditions problem is shown in Table I. In order to acquire the numerical solution of the defined optimal control problem using the pseudo-spectral method at each independent initial position, the initial airspace should be sampled. After obtained the numerical solutions of each position, the safe recovery flight envelope can be generated by data fitting.

TABLE I
ALGORITHM OF SOLVING THE REACHABILITY CONDITIONS PROBLEM

Require: The aircraft model, boundary constraints, control constraint, initial airspace Ω, number of samples n.
1: Initialize state constraints, boundary constraints, control constraint and airspace Ω.
2: Sample initial positions $(x_0^{(i)}, h_0^{(i)})_{i=1}^n$ from initial airspace Ω.
3: Solving the optimal control problem as in Section 3 for every initial position $(x_0^{(i)}, h_0^{(i)})$ by utilizing GPOPS toolbox, the numerical solutions $(u_{r\max}^{(i)})_{i=1}^n$ and $(u_{r\min}^{(i)})_{i=1}^n$ are obtained.
4: Fit the numerical solutions to get the minimum speed envelope as well as the maximum speed envelop.
5: Combine the minimum speed envelope and the maximum speed envelop to get the reachability conditions region.

A. The minimum speed envelope

With the purpose of solving minimum speed, consider the cost functional (13), control constraint(14) and boundary conditions (15)(16). The whole net recovery task is divided into three stages when solving the problem by GPOPS toolbox, namely at the start of the engine-shut-down stage, during the engine-shut-down stage and at the terminus of the engine-shut-down stage, and the constraints on states are different in these three stages.

Given the initial position (x_0, h_0) of the aircraft, on account of the fact that the maximum speed that Aerosonde UAV can reach is 20 m/s, the lower and upper limits on the state at the start of the engine-shut-down stage is given as

$$u_{r0} \in [0, 20] \tag{18}$$

The aircraft is in a state of gliding flight after the engine is shut down. Supposing that $w_r \in [-10, 10]$ m/s, $\theta \in [-1.05, 1.05]$ rad and $q \in [-1.2, 1.2]$ rad/s, then the lower and upper limits on the states during the engine-shut-down stage are given precisely:

$$\mathbf{x}_{\min} = [x_0 \quad 0 \quad 0 \quad -10 \quad -1.05 \quad -1.2]^T \tag{19}$$

$$\mathbf{x}_{\max} = [0 \quad h_0 \quad 20 \quad 10 \quad 1.05 \quad 1.2]^T \tag{20}$$

In addition, supposing that $w_r(t_f) = 0$, $\theta(t_f) \in [0, 0.7]$ rad and $q(t_f) \in [-1.2, 1.2]$ rad/s when the aerial vehicle is close to the recovery net and the size of net is $2m \times 2m$ namely $\varepsilon = 2$, then the lower and upper limits on the states at the terminus of the engine-shut-down stage are given precisely:

$$\mathbf{x}_{f\min} = [-1 \quad -1 \quad 1 \quad 0 \quad 0 \quad -1.2]^T \tag{21}$$

$$\mathbf{x}_{f\max} = [1 \quad 1 \quad 1 \quad 0 \quad 0.7 \quad 1.2]^T \tag{22}$$

Finally, suppose the control constraint during the whole phase is

$$u \in \left[-\frac{\pi}{6}, \frac{\pi}{6}\right] \tag{23}$$

Using the toolbox GPOPS in MATLAB® to solve the numerical solution of this optimal problem, and to fit the obtained data additionally, the minimum speed envelope can be obtained shown in Fig. 5.

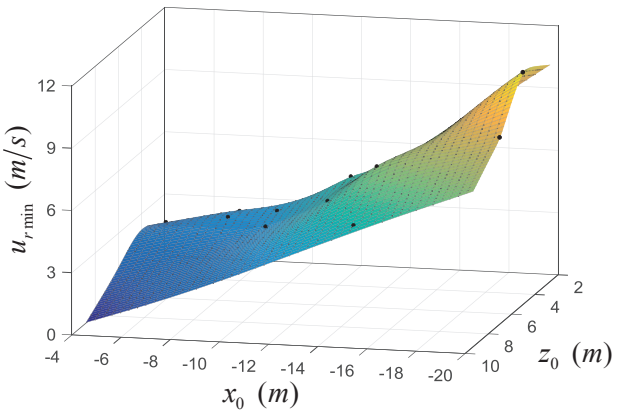

Fig. 5. The minimum speed envelope

B. The maximum speed envelope

With the purpose of solving maximum speed at the different initial position, consider the cost functional (17). Similar to solve the minimum speed envelope, constraints on states in three stages are same as expressions (18)-(22) and control constraint is same as expressions (23). Using the same method as solving the minimum speed envelope, the maximum speed envelope can be obtained shown in Fig. 6.

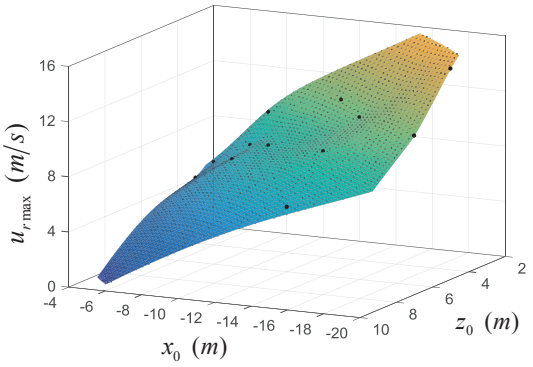

Fig. 6. The maximum speed envelope

C. The reachability conditions region

As described above, the reachability conditions are the flight envelope established by the maximum speed envelope and the minimum speed envelope. Therefore, showing the minimum speed envelope and the maximum speed envelope in one coordinate system, then the three-dimensional region defined by x_0-z_0-u_r between the two envelopes satisfies reachability conditions for safe recovery (Fig. 7). Only the case that points belong to the region probably perform net recovery successfully. Both the points above the maximum speed envelope and below the minimum speed envelope do not satisfy the reachability conditions. In other words, it is prone to failure.

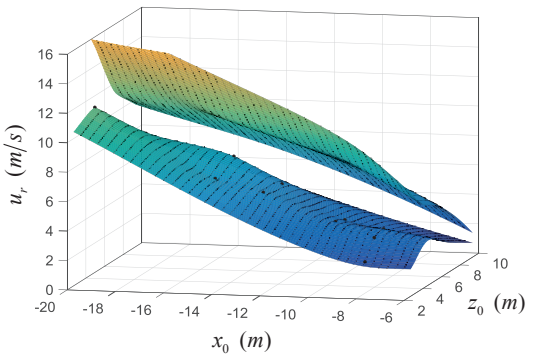

Fig. 7. The reachability conditions for safe recovery

V. Verification

For the sake of validating the accuracy of the result, some points from the reachability conditions region are randomly acquired to verify whether these points can reach the recovery net successfully. Therefore, consider the following optimal control problem. Minimize the cost functional

$$J = \int_{t_0}^{t_f} u(t)^2 dt \tag{24}$$

subject to dynamic constraint (1) and boundary conditions (15). Here, $u(t)$ represents control variable of the nonlinear dynamic model. The constraints on the state at the start of the phase is given as

$$\mathbf{x}_0 = [x_0 \ u_{r0} \ h_0 \ 0 \ 0 \ 0]^T \tag{25}$$

The lower and upper limits on the states during the stage are same as expressions (19) (20). The lower and upper limits on the states at the terminus of the stage are same as mathematical expressions (21) (22), as well as the control constraint during the whole phase is same as mathematical expression (26). *100* sets of data are tested by using the toolbox GPOPS to solve the numerical solutions of this optimization problem, and results show that *81* sets of data can perform successful net-recovery task, which means that most of the points are to meet the requirements under this control strategy. By the way, the failed test points maybe perform successful net-recovery task under other control strategies. The statistic results are shown as follow:

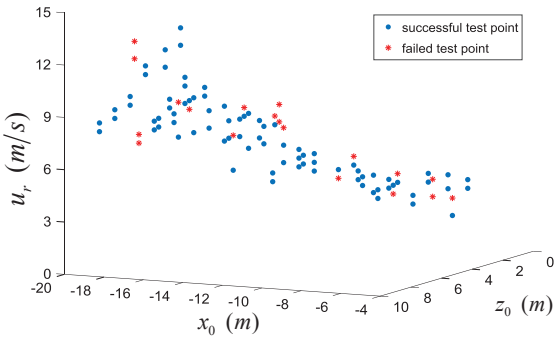

Fig. 8. Statistics of tested points

In order to be more representative, three cases are considered, including the point on the minimum speed envelope, the point on the maximum speed envelope and the point between the two envelopes, respectively. The selected points which performed successful net-recovery task are shown in Table II.

TABLE II
TESTED POINTS FROM REACHABILITY CONDITIONS REGION

	$Case1$	$Case2$	$Case3$
x_0	-8	-15	-9
h_0	3	5	4
u_{r0}	2.07	11.04	5.0

The simulation results are shown as follows:

A. Case 1: the point on the minimum speed envelope

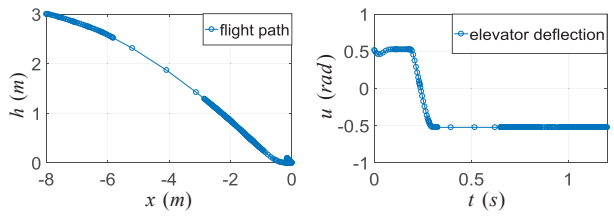

Fig. 9. The result of Case 1

B. Case 2: the point on the maximum speed envelope

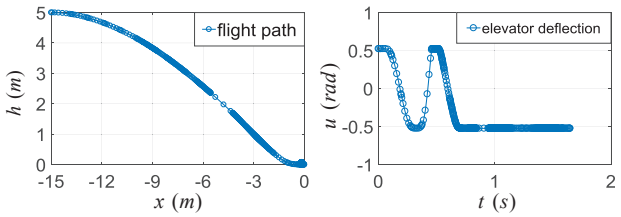

Fig. 10. The result of Case 2

C. Case 3: the point between the two envelopes

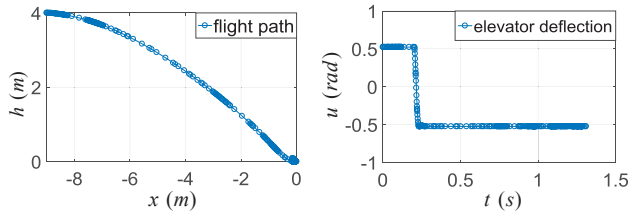

Fig. 11. The result of Case 3

It can be observed that the flight vehicle can reach the target point successfully, and the flight path is smooth enough. In other words, the results demonstrate that our method is effective. In addition, the results also show the change of control variable namely the elevator deflection, which reflects good maneuverability.

VI. Conclusion

In this paper, we have discussed the reachability conditions that UAVs should satisfy for net recovery, namely the constraint on speed. Given the initial position, the appropriate initial speed envelope is our target. A longitudinal dynamic model of the aerial vehicle is established at first. In addition, the problem is established as an optimal control problem and then successfully solved based on pseudo-spectral methods by utilizing GPOPS toolbox. Further, we obtained the reachability conditions region for safe recovery and the simulation results demonstrated it is valid and reasonable. This study, therefore, represents an approach to evaluate reachability conditions for recycling small fix-wing UAVs and the significant theoretical and practical value in net recovery have been demonstrated. The proposed method can have another application. For instance, SAIC and ArcXeon presented a concept of utilizing an airship as an airborne carrier for UAVs [14]. The reachability of these unmanned aircraft needs to be studied as well.

The method proposed in this paper can provide safety assessment for UAVs net recovery. However, some limitations are worth noting.The model did not take external disturbance into account such as wind. In future work, these will be taken into consideration.

Acknowledgment

The financial supports from the National Natural Science Foundation of China (61603014) for this work are greatly acknowledged.

References

[1] H. J. Kim, M. Kim, H. Lim et al., "Fully Autonomous Vision-Based Net-Recovery Landing System for a Fixed-Wing UAV", *IEEE/ASME Trans. on Mechatronics,* vol. 18, no. 4, pp. 1320-1333, Aug. 2013.

[2] S. Yoon, Y. Kim and S. Kim, "Pursuit Guidance Law and Adaptive Backstepping Controller Design for Vision-Based Net-Recovery UAV", presented at the AIAA Guidance Navigat. Contr. Conf., Honolulu, HI, USA, Aug. 2008.

[3] R. Skulstad, C. Syversen, M. Merz et al., "Autonomous Net Recovery of Fixed-Wing UAV with Single-Frequency Carrier-Phase Differential GNSS", *IEEE Aerosp. Electron. Syst. Mag.,* vol. 30, no. 5, pp. 18-27, May 2015.

[4] M. Dekel and J. Z. Ben-Asher, "Pseudo-Spectral-Method Based Optimal Glide in the Event of Engine Cut-off," presented at the AIAA Guidance Navigat. Contr. Conf., Portland, OR, USA, Aug. 2011.

[5] G. Elnagar, M. Kazemi, and M. Razzaghi, "The Pseudospectral Legendre Method for Discretizing Optimal Control Problems", *IEEE Trans. Autom. Control,* vol. 40, no. 10, pp. 1793-1796, Oct. 1995.

[6] F. Fahroo, and I. M. Ross, "Costate Estimation by a Legendre Pseudospectral Method", *J. Guid. Control Dyn.*, vol. 24, no. 2, pp. 270-277, 2001.

[7] S. Kameswaran, and L. T. Biegler, "Convergence Rates for Direct Transcription of Optimal Control Problems Using Collocation at Radau Points", *Comput. Optim. Appl.,* vol. 41, no. 1, pp. 81- 126, Sep. 2008.

[8] A. V. Rao, D. A. Benson, C. L. Darby et al., "GPOPS: A MATLAB Software for Solving Multiple-Phase Optimal Control Problems Using the Gauss Pseudospectral Method", *ACM Trans. Math. Softw.,* vol. 37, no. 2, pp. 22-39, 2010.

[9] D. A. Benson, G. T. Huntington, T. P. Thorvaldsen and A. V. Rao, "Direct Trajectory Optimization and Costate Estimation via an Orthogonal Collocation Method" , *J. Guid. Control Dyn.,* vol. 29, no. 6, pp. 1435-1440, Nov. 2006.

[10] D. Garg, M. A. Patterson, C. L. Darby et al., "Direct Trajectory Optimization and Costate Estimation of Finite-Horizon and Infinite-Horizon OptimalControl Problems Using a Radau Pseudospectral Method," *Comput. Optim. Appl.,* vol. 49, no. 2, pp. 335-358, 2011.

[11] D. Garg, M. A. Patterson, W. W. Hager et al., "A Unified Framework for the Numerical Solution of Optimal Control Problems Using Pseudospectral Methods", *Automatica,* vol. 46, no. 11, pp. 1843-1851, Jun. 2010.

[12] D. Garg, W. W. Hager, and A. V. Rao, "Pseudospectral Methods for Solving Infinite-Horizon Optimal Control Problems", *Automatica,* vol. 47, no. 4, pp. 829-837, Apr. 2011.

[13] R. W. Beard and T. W. McLain, *Small Unmanned Aircraft: Theory and Practice,* Princeton Univ. Press, Princeton, NJ, 2012.

[14] R. D. Hochstetler, J. Bosma, G. H. Chachad and M. L. Blanken, "Lighter-Than-Air (LTA) 'AirStation' Unmanned Aircraft System (UAS) Carrier Concept", presented at the 10th AIAA Aviation Technol. Integ. Oper. Conf., Washington, D.C., USA, Jun. 2016.